Electronic Supplementary Material (ESI) for Inorganic Chemistry Frontiers.

Supporting Information

Improving Catalysis for Electrochemical Water Splitting Using Phosphosulphide Surface

Lisi Yin,[a] Xinran Ding,[a] Wenxian Wei,[b] Yihui Wang,[a] Zizheng Zhu,[a] Kai Xu,[a] Ziming Zhao,[a] Hong Zhao,[a] Tingting Yu[a] and Tao Yang[,a]*

[a]Jiangsu Key Laboratory of Marine Bioresources and Environment, Co-Innovation Center of Jiangsu Marine Bio-industry Technology, Jiangsu Ocean University, Lianyungang 222005, China.

[b]Testing Center, Yangzhou University, Yangzhou 225009, China.

CORRESPONDING AUTHOR

Correspondence and requests for materials should be addressed to Tao Yang (yangtao_hit@163.com)

Experimental Section

Materials

All chemicals are of analytical grade and were used as received without further purification. Cobalt (II) acetate (99.99 %), nickel (II) nitrate hexahydrate (99.99 %), potassium ferricyanide (99.95 %), trisodium citrate dehydrate (99 %), sublimed sulfur (99.95 %), ammonium tetrathiomolybdate (99.95 %) and DMF (99.8 %) were purchased from Aladdin Industrial Corporation.

Synthesis of FeCoNi-PBA particles

Cobalt (II) acetate (320 mg), nickel (II) nitrate hexahydrate (525 mg) and trisodium citrate dihydrate (1600 g) were dissolved in water (120 mL). Potassium ferricyanide (800 mg) was dissolved in water (120 mL). The above two solutions were mixed uniformly after ultrasonic treatment (30 min) and then reacted in a water-bath at 28 ℃ for 20 h. The product, named as FeCoNi-PBA was then washed with water and ethanol for three times.

Synthesis of yolk-shell structured FeCoNi-S particles

FeCoNi-PBA (780 mg) and sublimed sulfur (55 mg) were dispersed in DMF (60 mL), then sealed in a Teflon-lined stainless-steel autoclave and reacted at 190 ℃ for 20 h. The product, named as FeCoNi-S was washed with ethanol for three times.

Synthesis of yolk-shell structured FeCoNi-PS particles

FeCoNi-S (100 mg) and $NaH_2PO_2 \cdot 2H_2O$ (1000 mg) were placed at two end positions of a quartz boat in a tube furnace. The furnace was heated at a heating rate of 2 °C min^{-1} and held at 320 ℃ for 2 h under argon flow. The phosphide product, named FeCoNi-PS

was obtained after cooling to ambient temperature. For comparison, FeCoNi-PBA was phosphated through the same process.

Characterization.

Morphologies of the products were measured on JEM-2100 TEM and a FEI apreo SEM. EDS spectroscopy was tested by using a TEM equipped with EDXA. Element distribution was performed on Tecnai-G2-F30 S-TWIN, which was equipped with HAADF detector. HRTEM and HAADF-STEM were observed on Talos F200x G2. The element in the near surface layers was demonstrated with XPS, which was demonstrated on ESCALAB 250Xi system. The PXRD spectrum of the samples were achieved on X'Pert PROM MPD (Panalytical) system with a CuK α X-ray sources (λ = 1.5406).

Preparation of samples for HER and OER electro-catalysis.

The catalyst slurry was prepared by mixing active material (1 mg) with pure carbon (Vulcan XC72, 1 mg) in a mixed solution of water (0.65 mL), ethanol (0.3 mL) and Nafion (5 % w/w in water and 1-propanol, 50 μL) with stirring.[1] A drop of the catalyst slurry (10 μL) was transferred onto a rotating disk electrode (RDE, 0.196 cm^2) with a pipette. After drying in airflow, the electrode was used for HER and OER test. As to the carbon paper electrodes, the carbon paper (1.0 ×1.0 cm^2) was repeatedly immersed into the catalyst slurry and dried in airflow. The net weight of the catalyst on the carbon paper was 1.5 mg. After drying in airflow, the carbon paper electrodes were used as both anode and cathode for the overall water splitting test.

Electrochemical characterizations.

HER and OER electro-catalysis tests were performed in a typical three-electrode configuration on PGSTAT-302N instrument. RDE with active sample was used as the

working electrode, Hg/HgO as the reference electrode and a Pt foil (1.0 cm^2) as the counter electrode. All of the polarization curves were measured in 1.0 M KOH solution by using RDE with a rotation of 1600 r.p.m. at a scan rate of 5 mVs^{-1}. The electrochemical double-layer capacitance was used as an indicator for ECSA. Cyclic voltammetry was carried out at six different scan rates of 10, 20, 40, 80, 120 and 160 mV s^{-1}. Absolute value of the measured capacitive current densities at the average potential in the selected range were added and plotted as a function of the scan rates, the slope of the linear fit was used as an indicator for ECSA. Overall water splitting was tested in a two-electrode system by using the carbon paper electrodes as both the cathode and anode at 1.8 V, the current density vs. time was plotted. To simplify the calculation, TOF of HER and OER was calculated based on the catalysts mass. For HER, the TOF is:

$$TOF_{HER} = \frac{Jt}{2mF} \quad (1)$$

For OER, the TOF is

$$TOF_{OER} = \frac{Jt}{4mF} \quad (2)$$

J is the current on the electrodes, A;

t is 3600 s,

m is the mass of catalyst, g;

F is Fraraday Constant, 96485.

Thus, the unit of TOF is $g^{-1}h^{-1}$.

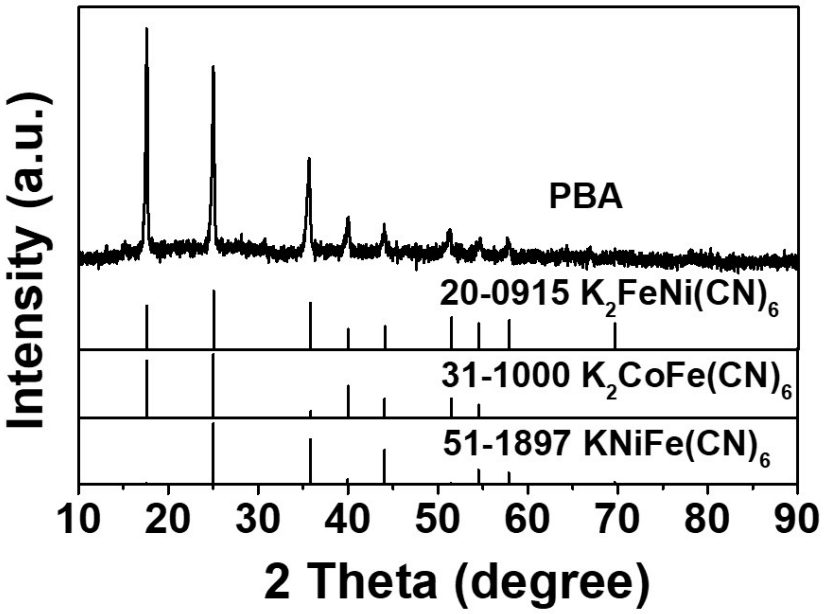

Fig. S1 XRD pattern of FeCoNi-PBA. The standard patterns of $K_2FeNi(CN)_6$, $K_2CoFe(CN)_6$ and $KNiFe(CN)_6$ are also plotted for reference.

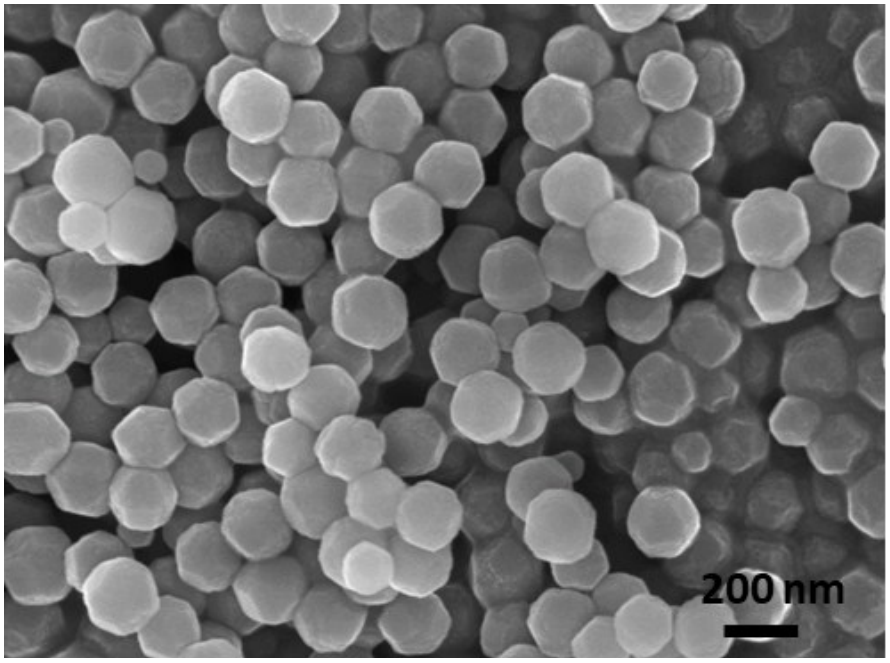

Fig. S2 SEM image of FeCoNi-PBA. The as-obtained FeCoNi-PBA are dominantly polyhedral shape with rough edges and corners.

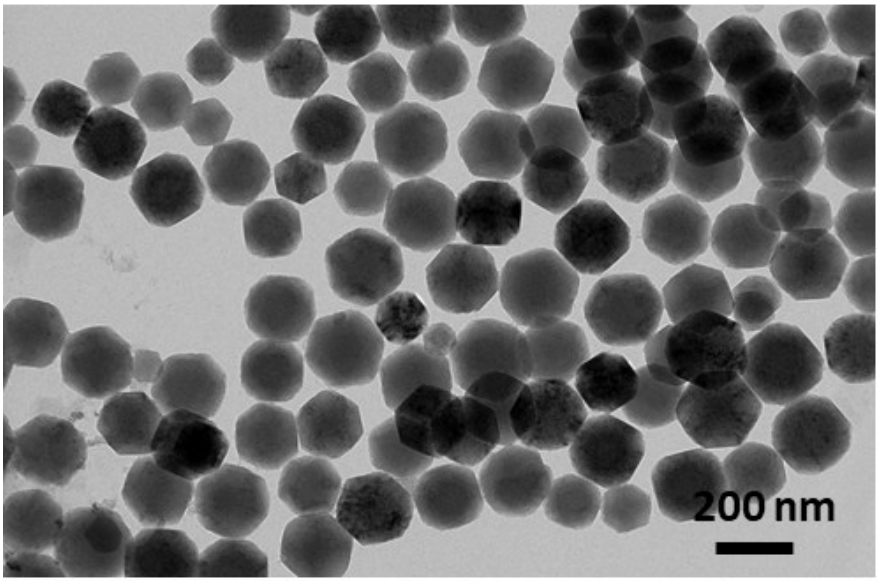

Fig. S3 TEM image of FeCoNi-PBA. The as-obtained FeCoNi-PBA are dominantly polyhedral shape with rough edges and corners.

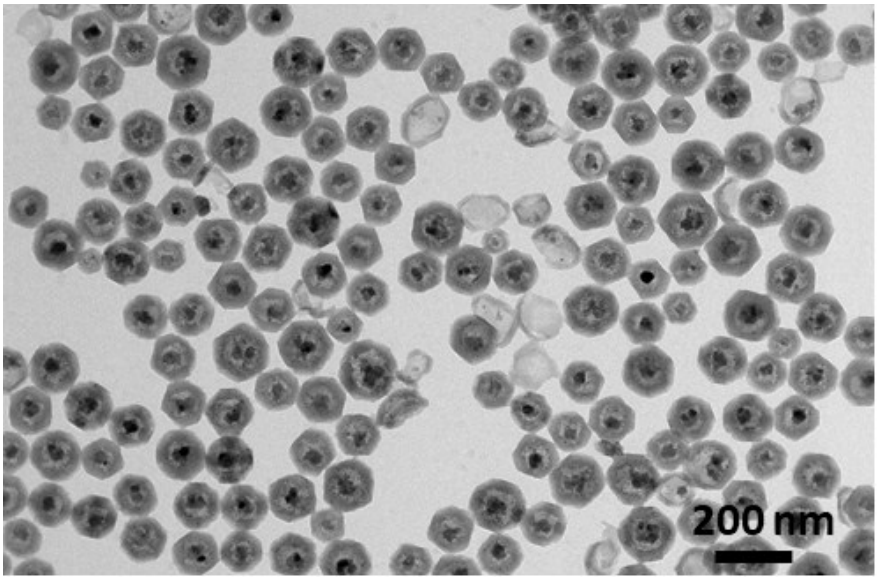

Fig. S4 TEM image of FeCoNi-S. The FeCoNi-S are mainly yolk-shell structure.

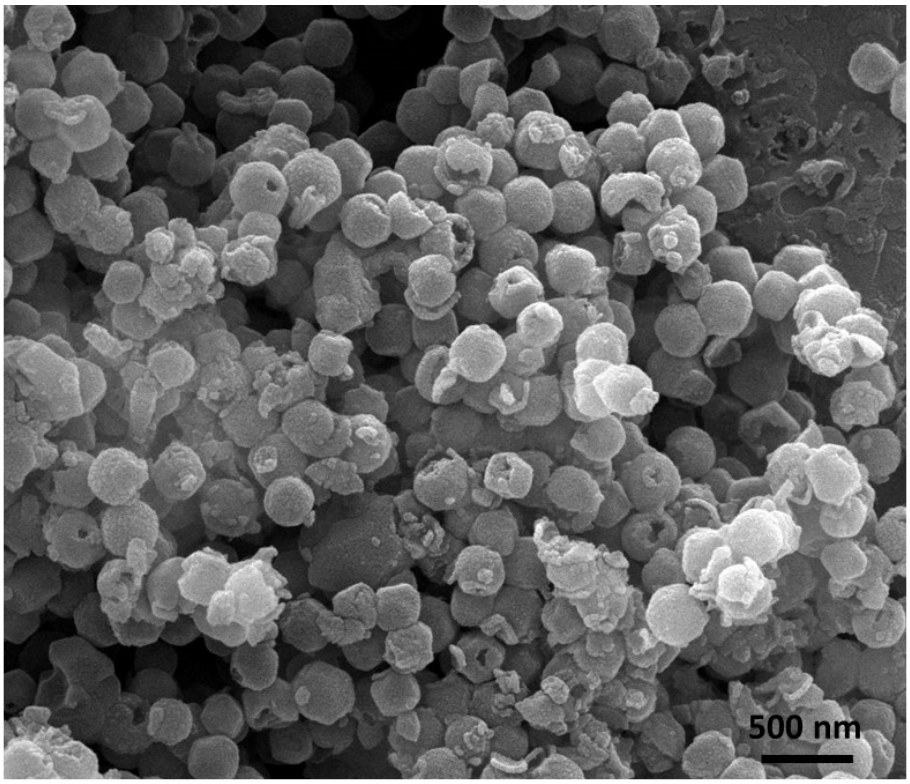

Fig. S5 SEM image of FeCoNi-PS. Compared with FeCoNi-S, some of the phosphatized products show openings and become more rounded.

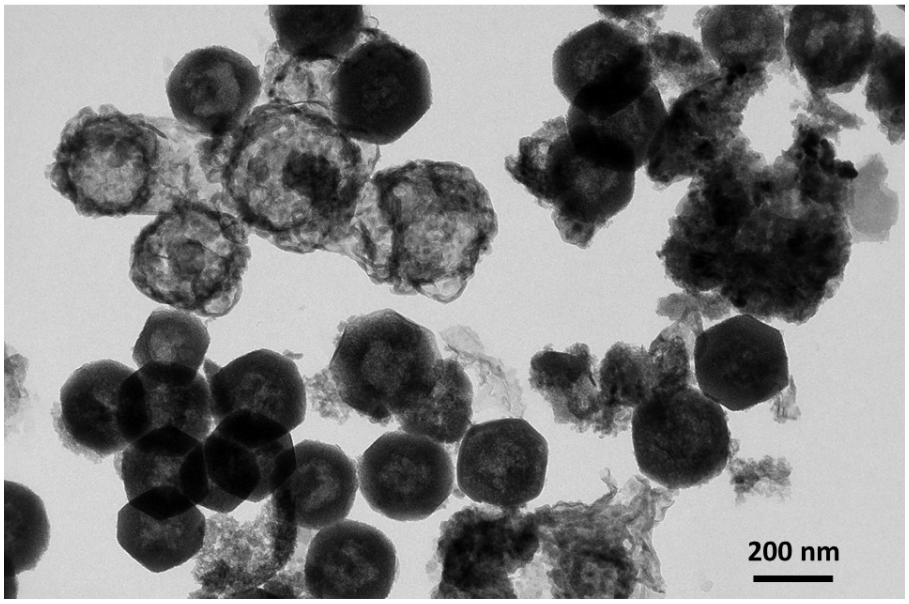

Fig. S6 TEM image of FeCoNi-PS. Most of the particles inherit yolk-shell structure from FeCoNi-S.

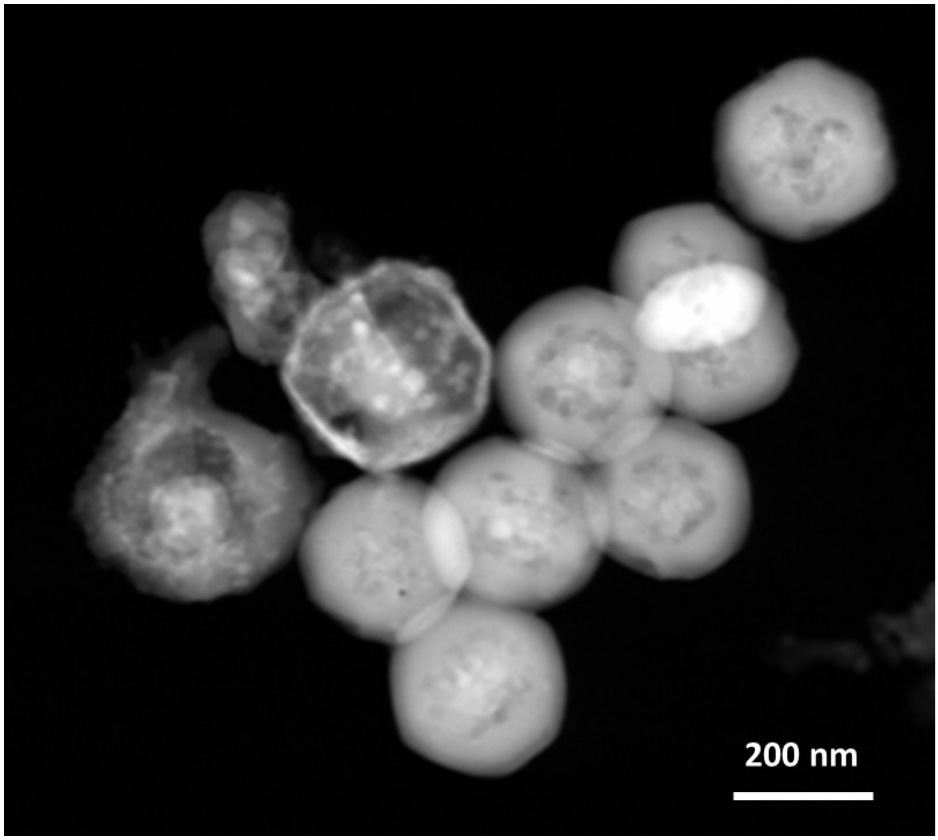

Fig. S7 HAADF-STEM of FeCoNi-PS. HADDF-STEM images show the difference in brightness, suggesting a uniform structure.

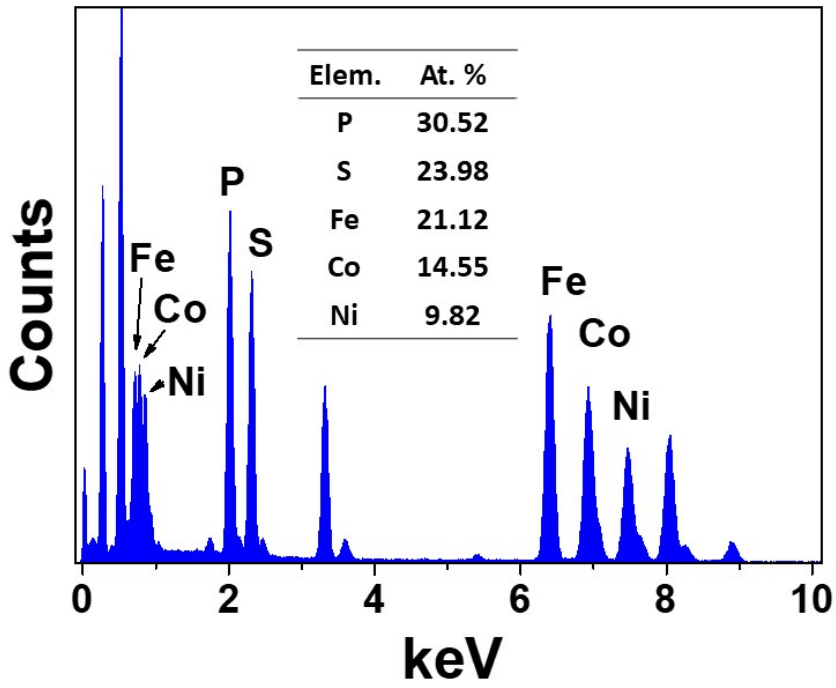

Fig. S8 TEM-EDX spectra of FeCoNi-PS.

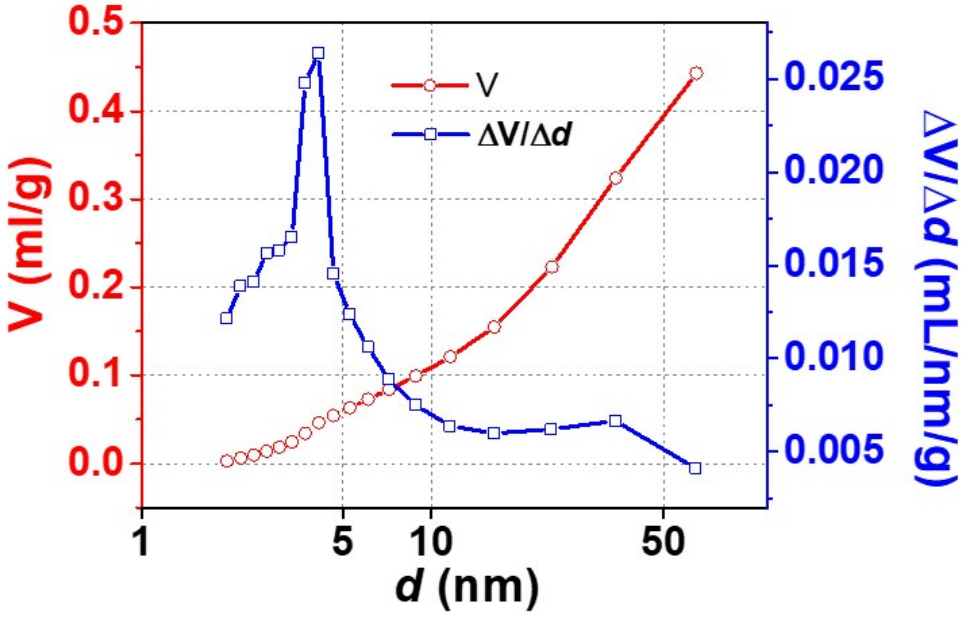

Fig. S9 Pore diameter distribution of FeCoNi-PS. The most probable pore diameter is 3.91 nm.

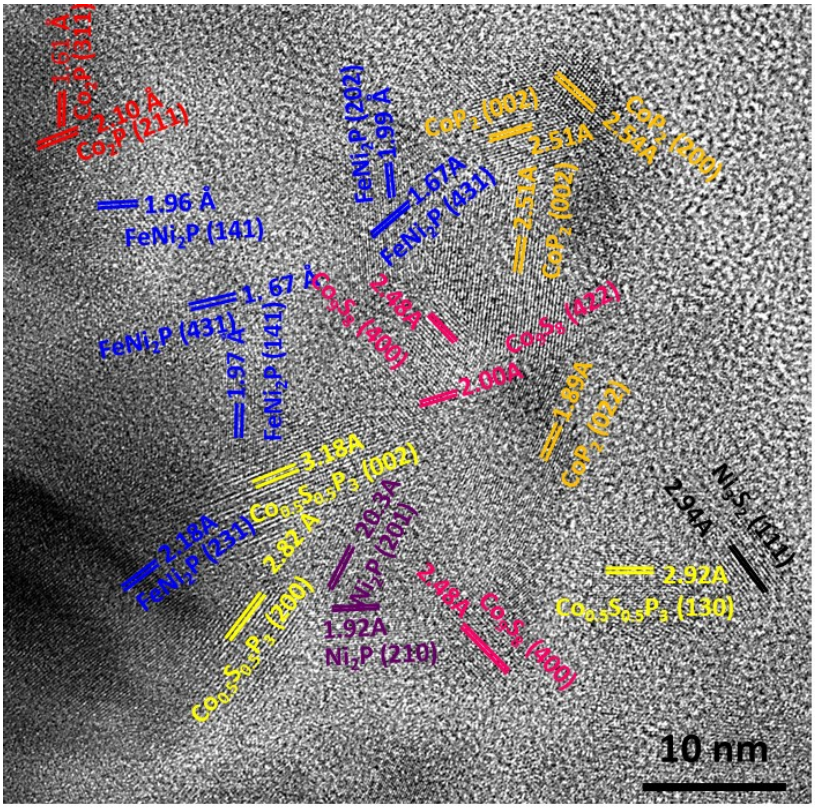

Fig. S10 HRTEM image of FeCoNi-PS. The distinct lattice fringes can be observed, well triggered to sulphides, phosphides, and $Co_{0.5}S_{0.5}P_3$.

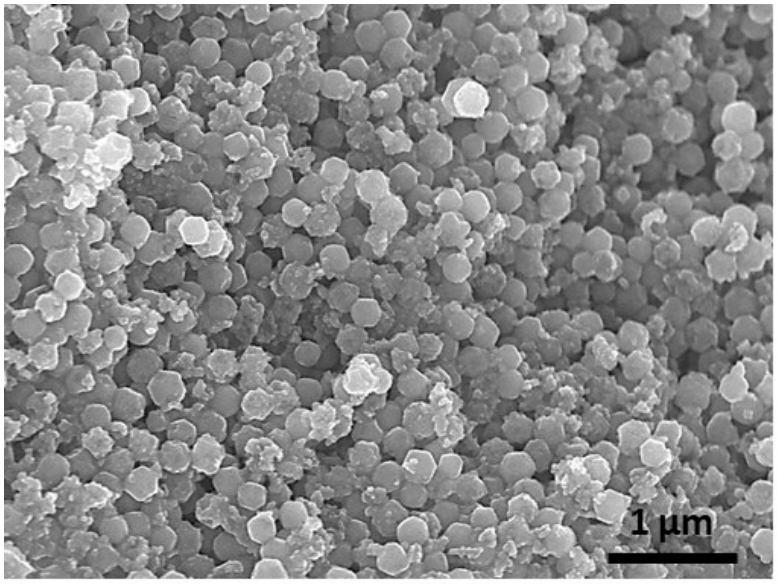

Fig. S11 SEM image of FeCoNi-P.

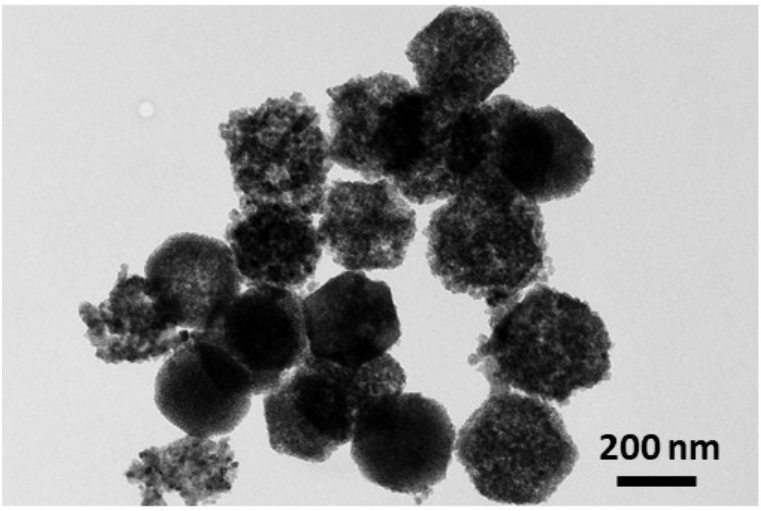

Fig. S12 TEM image of FeCoNi-P.

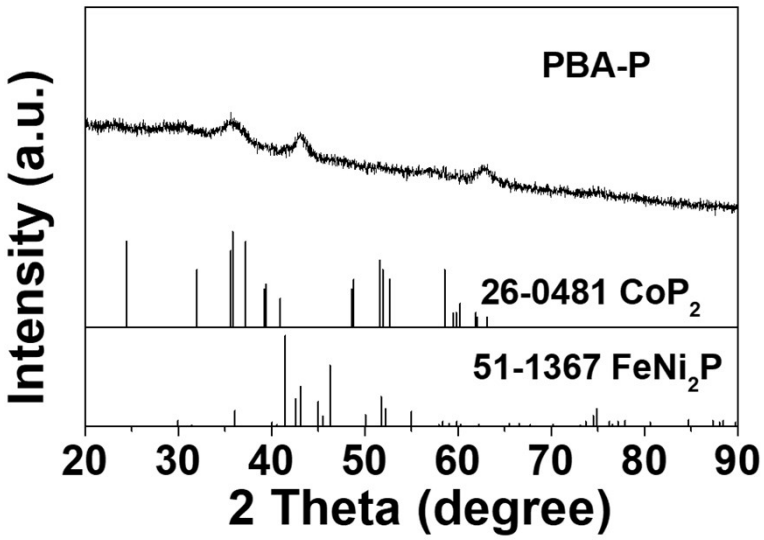

Fig. S13XRD pattern of FeCoNi-P.

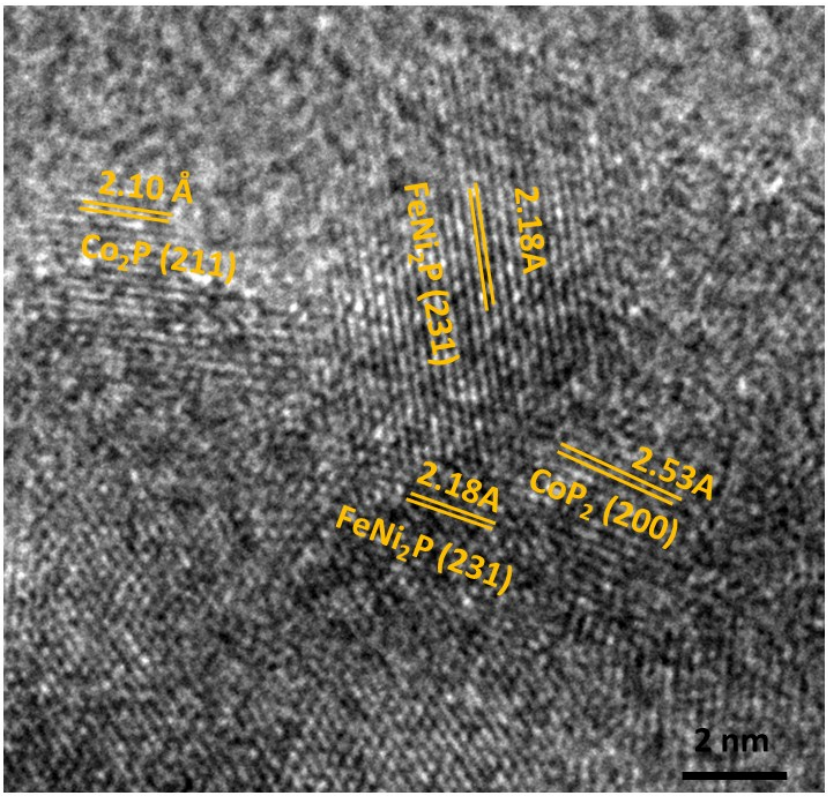

Fig. S14 HRTEM image of FeCoNi-P.

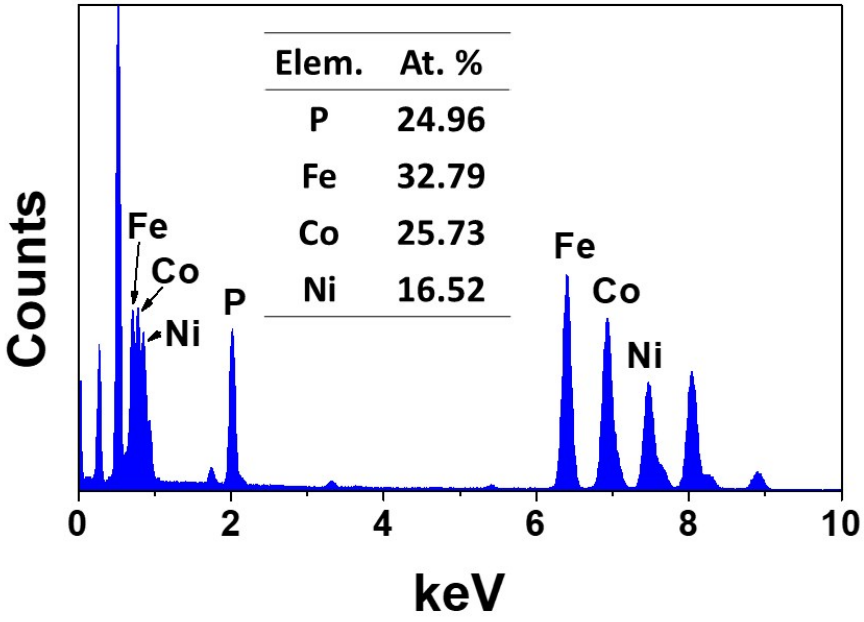

Fig. S15 TEM-EDX spectra of FeCoNi-P.

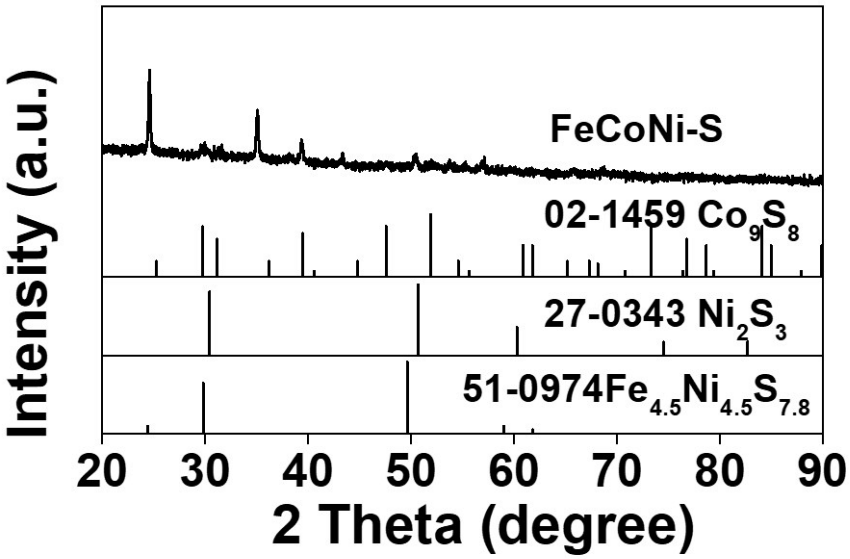

Fig. S16 XRD pattern of FeCoNi-S.

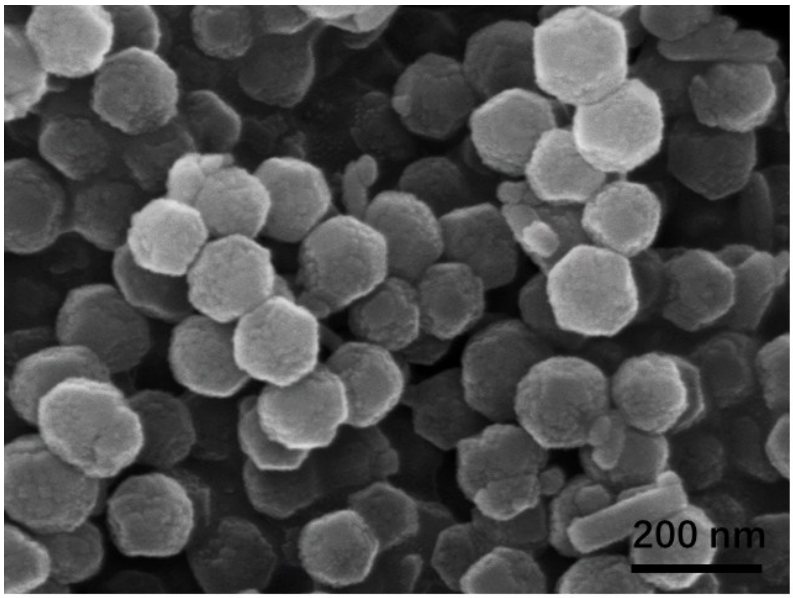

Fig. S17 SEM image of FeCoNi-S.

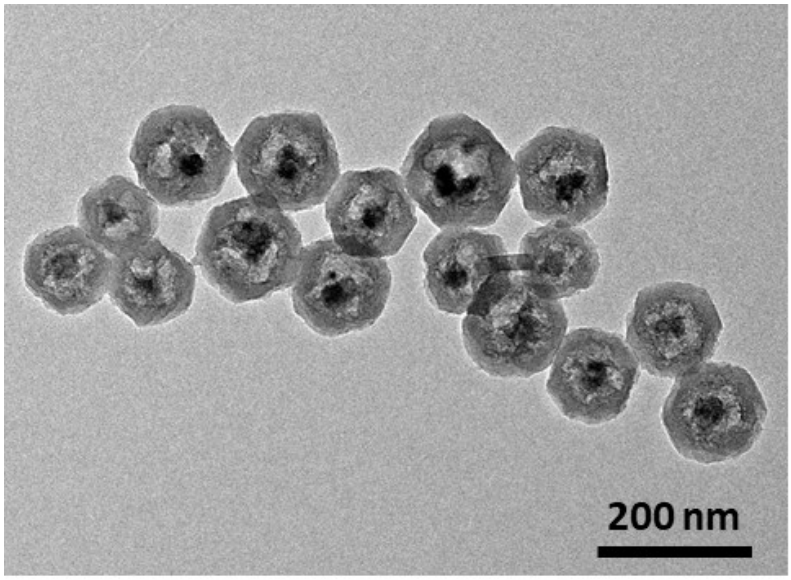

Fig. S18 TEM image of FeCoNi-S.

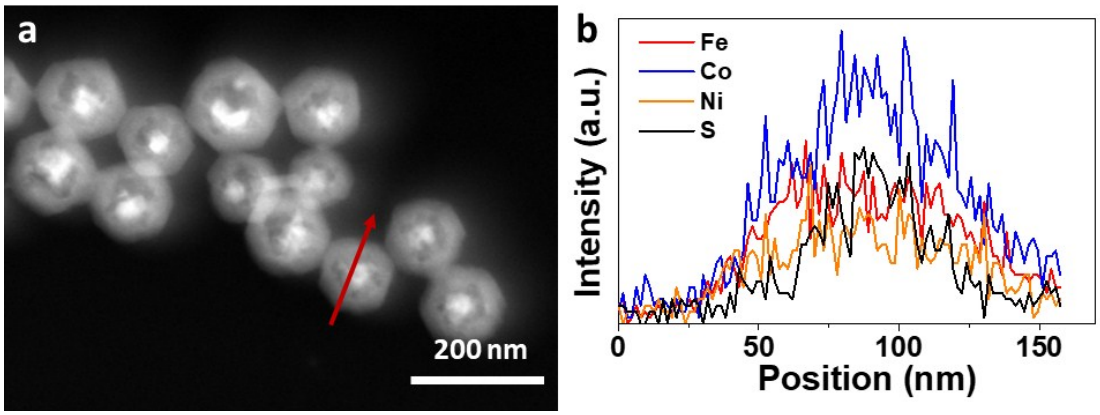

Fig. S19 (a) HAADF-STEM image of FeCoNi-S and (b) EDX cross-sectional line profile on an individual particle.

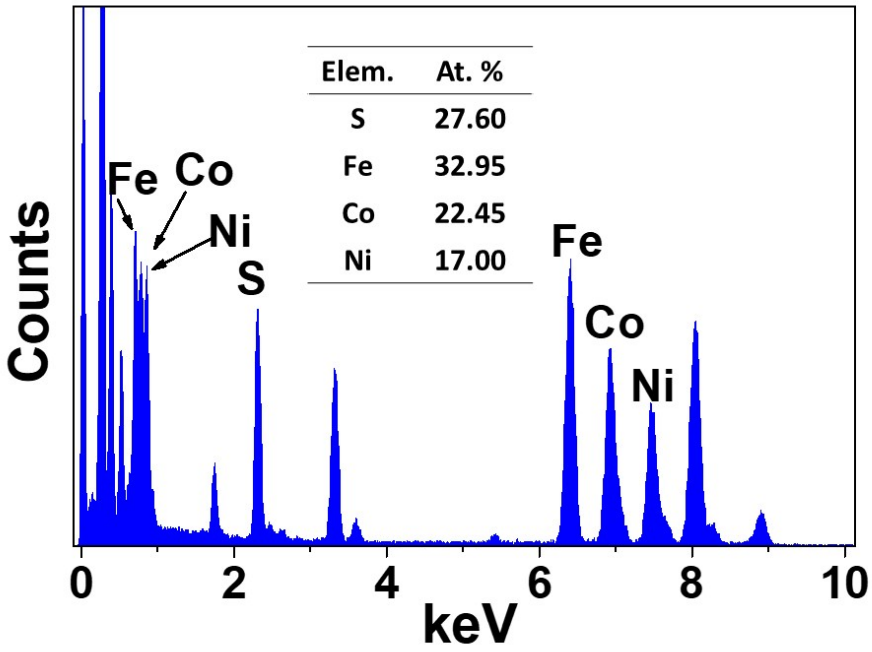

Fig. S20 TEM-EDX spectra of FeCoNi-S. The atomic ratio of Fe, Co, Ni and S has been presented.

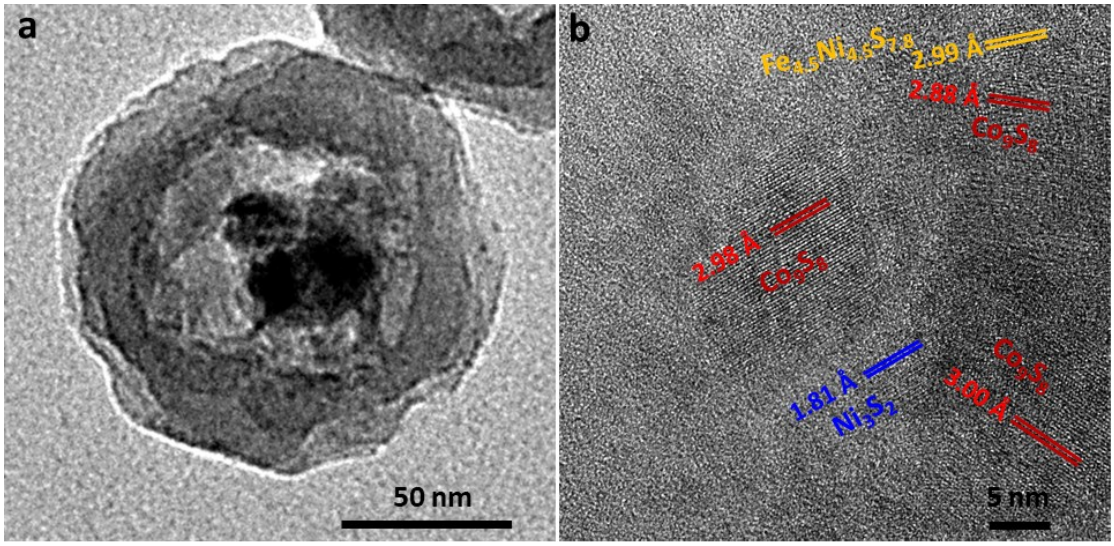

Fig. S21 (a) TEM and (b) HRTEM images of FeCoNi-S. The lattice fringes correspond to the planes of Co_9S_8, Ni_3S_2 and $Fe_{4.5}Ni_{4.5}S_{7.8}$, respectively.

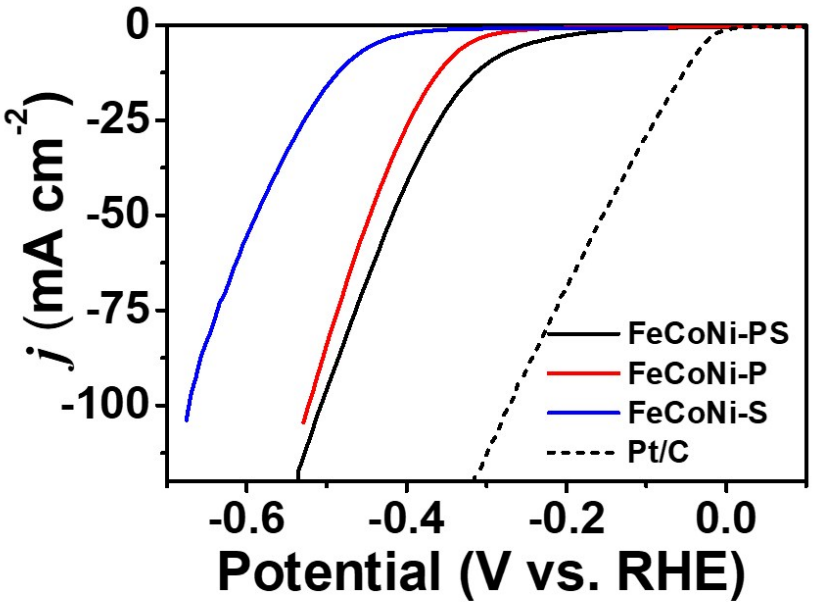

Fig. S22 Polarization curves of FeCoNi-PS, FeCoNi-P, FeCoNi-S and commercial Pt/C for HER without iR correction.

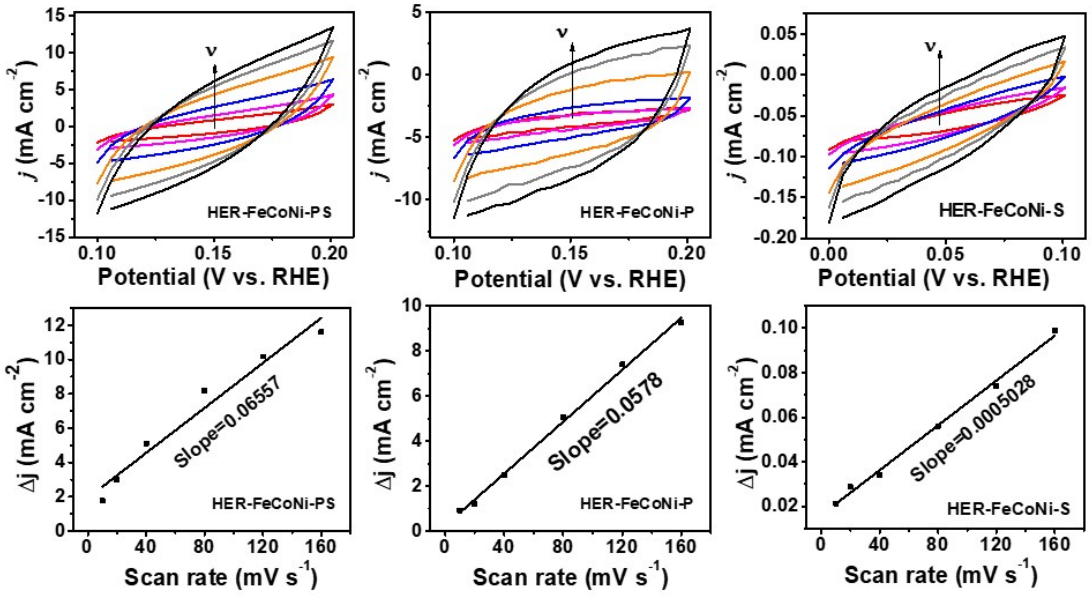

Fig. S23 Double-layer capacitances of FeCoNi-PS, FeCoNi-P and FeCoNi-S for HER.

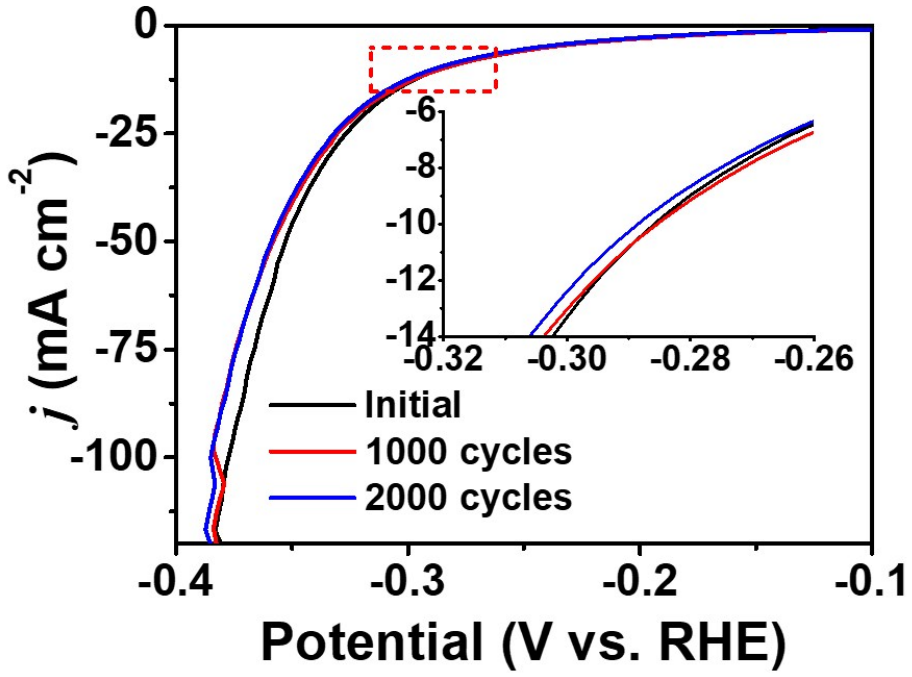

Fig. S24 Stability test of FeCoNi-PS. Inset is the enlarged region in the ranges of -0.32 ~ -0.26 V (vs. RHE) and -14 ~ -6 mA cm^{-2}.

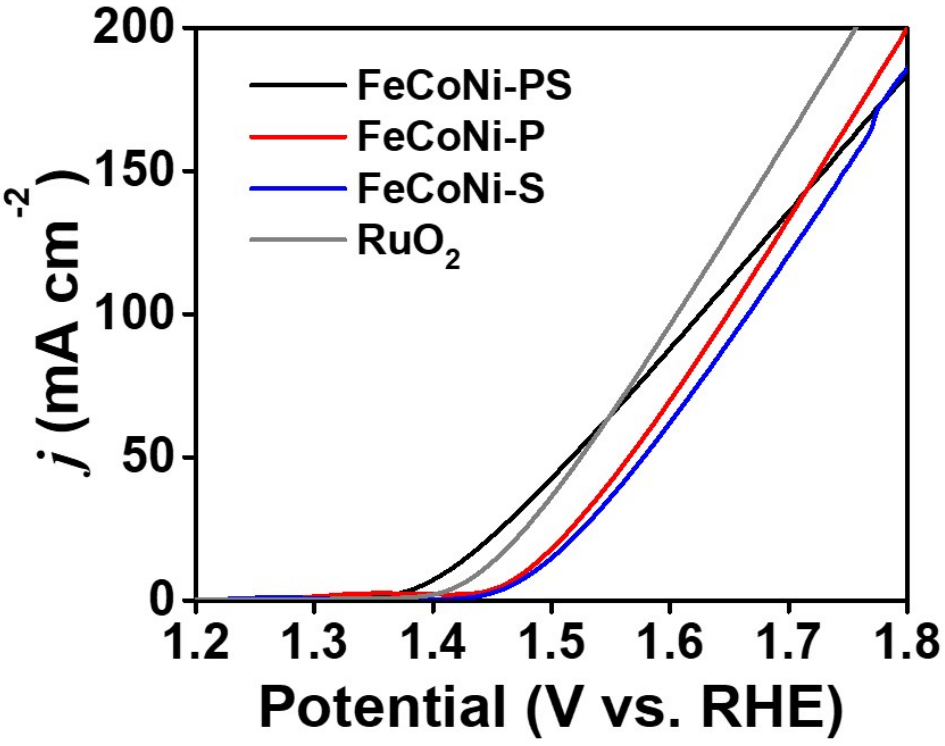

Fig. S25 Polarization curves of FeCoNi-PS, FeCoNi-P, FeCoNi-S and commercial RuO_2 for OER without iR correction.

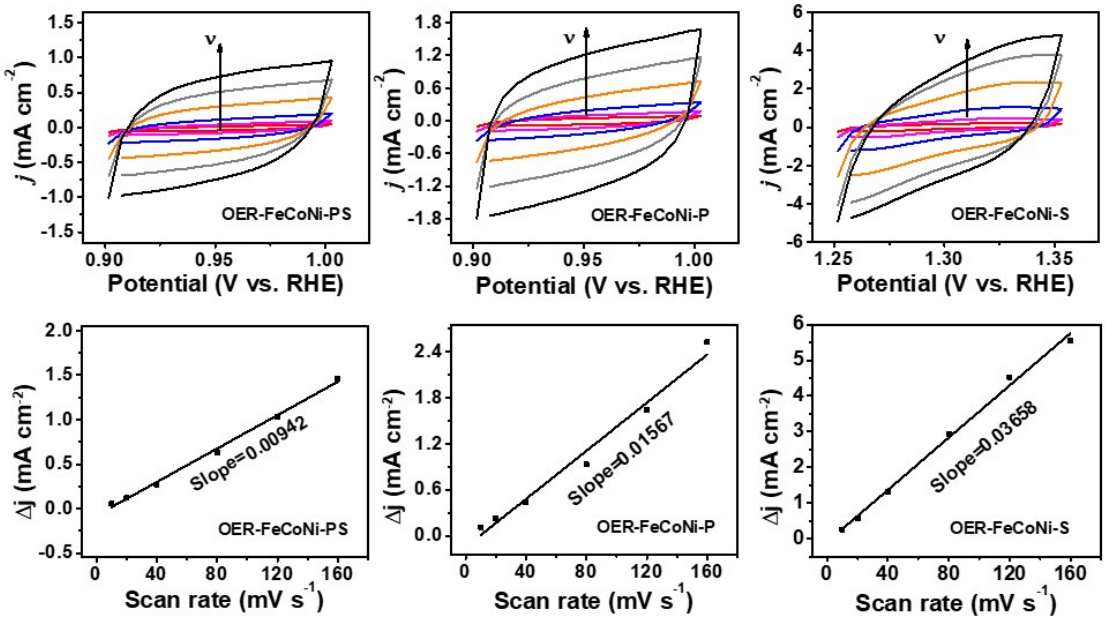

Fig. S26 Double-layer capacitances of FeCoNi-PS, FeCoNi-P and FeCoNi-S for OER. The scan rates were selected as 10, 20, 40, 80, 120 and 160 mV s^{-1}.

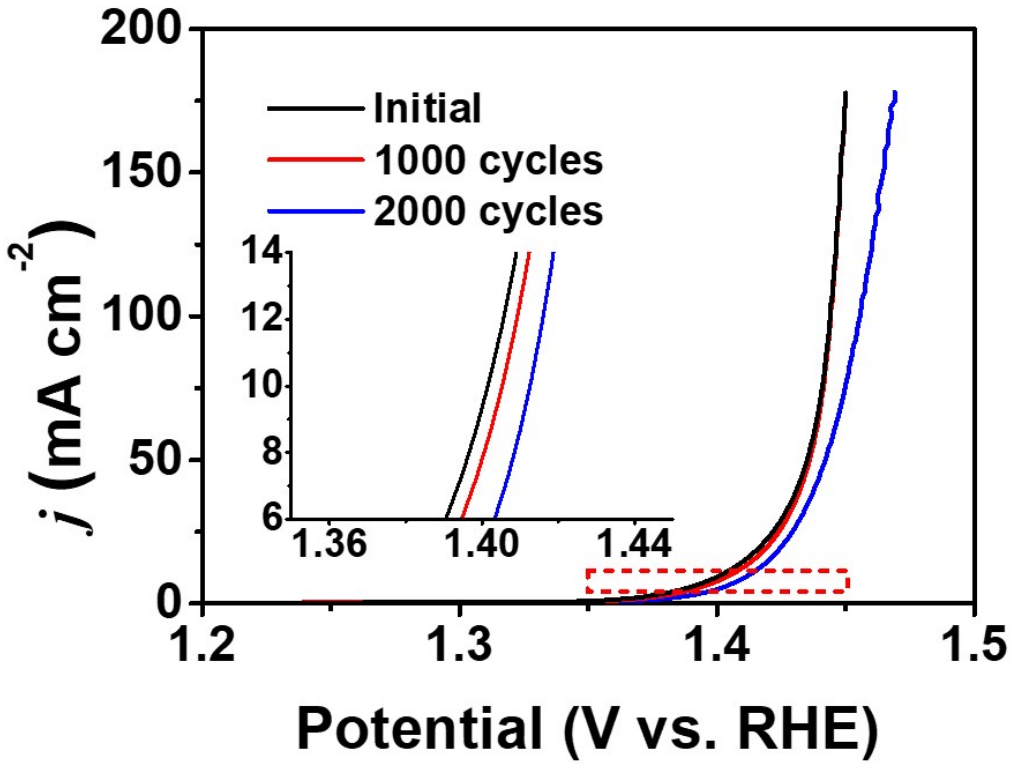

Fig. S27 Stability test of FeCoNi-PS for OER. Inset is the enlarged region in the ranges of 1.35-1.45 V (vs. RHE) and 6-14 mA cm^2.

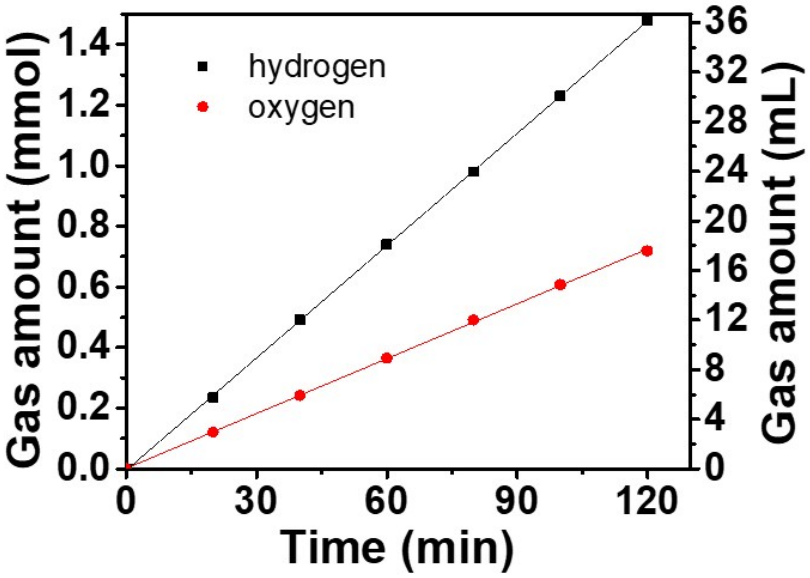

Fig. S28 The collected hydrogen and oxygen at a constant current density of 40 mA cm^{-2} at 298 K. The amount of hydrogen and oxygen shows a molar ratio of 2.04:1. The faradic efficiencies of HER and OER are 99.3 % and 97.1 %, respectively.

Table S1 HER and OER overpotentials at 10 mA cm^{-2} in 1.0 M KOH

Catalysts	Over-potential (mV vs. RHE)		Ref.
	HER	OER	
FeCoNi-PS	284	162	This work
FeCoNi-P	346	235	This work
FeCoNi-S	468	244	This work
Co_9S_8	461	384	2
Co_9S_8@MoS_2/CNFs	-	430	3
Porous Co phosphide/Phosphate	380	-	4
Amorphous cobalt phosphosulfide on Ni foams	-	283	5
$NiCo_2S_4$ NWs/NF	-	260	6
CoP NSs	-	277	7
Ni-P	-	300	8
Co-Mn-P	-	330	9
Co-Fe-P 3D electrode	-	270	10
Ni_5P_4 films	-	290	11
Ni_2P	-	290	12
NiP/Ni	-	270	13
Ni_2P/Ni/NF	-	200	14
NiFe–NS	-	302	15
Co-P film	-	345	16
CoP-MNA	-	290	17
NiCoPS/CC	-	230	18
$NiP_{0.62}S_{0.38}$	-	240	19
NiCoP	-	280	20
NiCoFeP	-	273	21
CP/CTs/Co-S	-	306	22

FeP		350	23

References

1. Li, H.; Chen, S.; Jia, X.; Xu, B.; Lin, H.; Yang, H.; Song, L.; Wang, X., Amorphous nickel-cobalt complexes hybridized with 1T-phase molybdenum disulfide via hydrazine-induced phase transformation for water splitting. *Nat. Commun.* 2017, *8*, 15377.

2. Bai, J.; Meng, T.; Guo, D.; Wang, S.; Mao, B.; Cao, M., Co9S8@MoS2 Core–Shell Heterostructures as Trifunctional Electrocatalysts for Overall Water Splitting and Zn–Air Batteries. *ACS Appl. Mater. Interfaces* 2018, *10* (2), 1678-1689.

3. Zhu, H.; Zhang, J.; Yanzhang, R.; Du, M.; Wang, Q.; Gao, G.; Wu, J.; Wu, G.; Zhang, M.; Liu, B.; Yao, J.; Zhang, X., When Cubic Cobalt Sulfide Meets Layered Molybdenum Disulfide: A Core–Shell System Toward Synergetic Electrocatalytic Water Splitting. *Adv. Mater.* 2015, *27* (32), 4752-4759.

4. Yang, Y.; Fei, H.; Ruan, G.; Tour, J. M., Porous Cobalt-Based Thin Film as a Bifunctional Catalyst for Hydrogen Generation and Oxygen Generation. *Adv. Mater.* 2015, *27* (20), 3175-3180.

5. Du, F.; Zhang, Y.; He, H.; Li, T.; Wen, G.; Zhou, Y.; Zou, Z., Electrodeposited amorphous cobalt phosphosulfide on Ni foams for highly efficient overall water splitting. *J. Power Sources* 2019, *431*, 182-188.

6. Sivanantham, A.; Ganesan, P.; Shanmugam, S., Hierarchical NiCo2S4 Nanowire Arrays Supported on Ni Foam: An Efficient and Durable Bifunctional Electrocatalyst for Oxygen and Hydrogen Evolution Reactions. *Adv. Funct. Mater.* 2016, *26* (26), 4661-4672.

7. Chang, J.; Liang, L.; Li, C.; Wang, M.; Ge, J.; Liu, C.; Xing, W., Ultrathin cobalt phosphide nanosheets as efficient bifunctional catalysts for a water electrolysis cell and the origin for cell performance degradation. *Green Chem.* 2016, *18* (8), 2287-2295.

8. Yu, X.-Y.; Feng, Y.; Guan, B.; Lou, X. W.; Paik, U., Carbon coated porous nickel phosphides nanoplates for highly efficient oxygen evolution reaction. *Energy Enviorn. Sci.* 2016, *9* (4), 1246-1250.

9. Li, D.; Baydoun, H.; Verani, C. N.; Brock, S. L., Efficient Water Oxidation Using CoMnP Nanoparticles. *J. Am. Chem. Soc.* 2016, *138* (12), 4006-4009.

10. Tan, Y.; Wang, H.; Liu, P.; Shen, Y.; Cheng, C.; Hirata, A.; Fujita, T.; Tang, Z.; Chen, M., Versatile nanoporous bimetallic phosphides towards electrochemical water splitting. *Energy Enviorn. Sci.* 2016, *9* (7), 2257-2261.

11. Ledendecker, M.; Krick Calderón, S.; Papp, C.; Steinrück, H.-P.; Antonietti, M.; Shalom, M., The Synthesis of Nanostructured Ni5P4 Films and their Use as a Non-Noble Bifunctional Electrocatalyst for Full Water Splitting. *Angew. Chem. Int. Ed.* 2015, *54* (42), 12361-12365.

12. Stern, L.-A.; Feng, L.; Song, F.; Hu, X., Ni2P as a Janus catalyst for water splitting: the oxygen evolution activity of Ni2P nanoparticles. *Energy Enviorn. Sci.* 2015, *8* (8), 2347-2351.

13. Chen, G.-F.; Ma, T. Y.; Liu, Z.-Q.; Li, N.; Su, Y.-Z.; Davey, K.; Qiao, S.-Z., Efficient and Stable Bifunctional Electrocatalysts Ni/NixMy (M = P, S) for Overall Water Splitting. *Adv. Funct. Mater.* 2016, *26* (19), 3314-3323.

14. You, B.; Jiang, N.; Sheng, M.; Bhushan, M. W.; Sun, Y., Hierarchically Porous Urchin-Like Ni2P Superstructures Supported on Nickel Foam as Efficient Bifunctional Electrocatalysts for Overall Water Splitting. *ACS Catal.* 2016, *6* (2), 714-721.

15. Song, F.; Hu, X., Exfoliation of layered double hydroxides for enhanced oxygen evolution

catalysis. *Nat. Commun.* 2014, *5* (1), 4477.
16. Jiang, N.; You, B.; Sheng, M.; Sun, Y., Electrodeposited Cobalt-Phosphorous-Derived Films as Competent Bifunctional Catalysts for Overall Water Splitting. *Angew. Chem. Int. Ed.* 2015, *54* (21), 6251-6254.
17. Zhu, Y.-P.; Liu, Y.-P.; Ren, T.-Z.; Yuan, Z.-Y., Self-Supported Cobalt Phosphide Mesoporous Nanorod Arrays: A Flexible and Bifunctional Electrode for Highly Active Electrocatalytic Water Reduction and Oxidation. *Adv. Funct. Mater.* 2015, *25* (47), 7337-7347.
18. Li, J.; Xia, Z.; Zhou, X.; Qin, Y.; Ma, Y.; Qu, Y., Quaternary pyrite-structured nickel/cobalt phosphosulfide nanowires on carbon cloth as efficient and robust electrodes for water electrolysis. *Nano Res.* 2017, *10* (3), 814-825.
19. Luo, J.; Wang, H.; Su, G.; Tang, Y.; Liu, H.; Tian, F.; Li, D., Self-supported nickel phosphosulphide nanosheets for highly efficient and stable overall water splitting. *J. Mater. Chem. A* 2017, *5* (28), 14865-14872.
20. Liang, H.; Gandi, A. N.; Anjum, D. H.; Wang, X.; Schwingenschlögl, U.; Alshareef, H. N., Plasma-Assisted Synthesis of NiCoP for Efficient Overall Water Splitting. *Nano Lett.* 2016, *16* (12), 7718-7725.
21. Guo, Y.; Tang, J.; Wang, Z.; Sugahara, Y.; Yamauchi, Y., Hollow Porous Heterometallic Phosphide Nanocubes for Enhanced Electrochemical Water Splitting. *Small* 2018, *14* (44), 1802442.
22. Wang, J.; Zhong, H.-x.; Wang, Z.-l.; Meng, F.-l.; Zhang, X.-b., Integrated Three-Dimensional Carbon Paper/Carbon Tubes/Cobalt-Sulfide Sheets as an Efficient Electrode for Overall Water Splitting. *ACS Nano* 2016, *10* (2), 2342-2348.
23. Xiong, D.; Wang, X.; Li, W.; Liu, L., Facile synthesis of iron phosphide nanorods for efficient and durable electrochemical oxygen evolution. *Chem. Commun.* 2016, *52* (56), 8711-8714.